ARTICLE

Electron Momentum Spectroscopy Investigation on Electronic Structure of Iso-dichloroethylene Valence Shell

Yi-chun Wang, Shan-shan Niu, Ya-guo Tang, Yu Zhang, Xu Shan, Chun-kai Xu*, Xiang-jun Chen

Hefei National Laboratory for Physical Sciences at the Microscale and Department of Modern Physics, University of Science and Technology of China, Hefei 230026, China

(Dated: Received on March 22, 2019; Accepted on April 29, 2019)

Here an electron momentum spectroscopy study on the electronic structure of valence shell of iso-dichloroethylene molecule is reported. The experiment is carried out with a binary (e, 2e) spectrometer at incident electron energy of 1200 eV, employing noncoplanar symmetric arrangement. The binding energy spectra and electron momentum distributions (EMDs) of iso-dichloroethylene valence shell have been obtained. Theoretical EMDs are predicted with both Hartree-Fock and density functional theory methods, generally indicating good agreements with the measurement results. The interference effect is observed to significantly influence the EMDs of $2a_2$ and $5b_2$ Cl lone-pair orbitals.

Key words: Electron momentum spectroscopy, Valence orbital, Lone-pair orbital, Interference effect

I. INTRODUCTION

Electron momentum spectroscopy (EMS), or binary (e, 2e) spectroscopy, is based on kinematically complete ionization experiments initiated by high energy electrons. In the past decades, it has been proven as a powerful technique for investigating both the binding energy spectra (BES) and the electron momentum distributions (EMDs) for individual atomic and molecular orbitals [1−7]. Such information helps us to evaluate the quality of different theoretical models for calculating electronic wave functions of atoms and molecules [1], as well as understand the relation between electron density distribution and chemical reactivity [8]. Iso-dichloroethylene (iso-$C_2H_2Cl_2$) is one of the three isomers of dichloroethylene, in which the two chlorine atoms are bound to the same carbon atom. Since it plays an important role as a common chlorine source for processing and treatment of silicon wafers in semiconductor material industry [9, 10], its electronic structure has been investigated extensively by electron energy loss spectra [9, 11], photoelectron spectra (including resonant Auger spectra) [12−18], X-ray absorption spectra [16−18], Penning ionization electron spectra [19], *etc.* The EMS study on iso-$C_2H_2Cl_2$ has also been performed by Chuaqui *et al.* [20]. However, only the EMDs for part of 12 valence orbitals were presented, including 3 outer-valence orbitals ($3b_1$, $10a_1$ and $6b_2$) and 4 inner-valence orbitals ($9a_1$, $8a_1$, $5b_2$ and $7a_1$). There remained an obvious discrepancy between the experiment and calculations.

In this work, we report an EMS study on the electronic structure of all the iso-$C_2H_2Cl_2$ valence orbitals. The experiment is performed by a high-sensitivity angle and energy dispersive multichannel electron momentum spectrometer at incident energy of 1200 eV plus the binding energy. Two-dimensional energy and azimuthal angle density map in the valence region have been measured, from which the BES as well as the EMDs of the iso-$C_2H_2Cl_2$ valence shell are obtained. Theoretical calculations are carried out using Hartree-Fock (HF) and density functional theory (DFT) methods within the framework of plane wave impulse approximation (PWIA). The interference effect is observed to significantly influence the EMDs of $2a_2$ and $5b_2$ orbitals, which consist of mainly Cl lone-pair electrons.

II. EXPERIMENTS

EMS experiment is based on the (e, 2e) process, in which a fast incident electron impacts with a target atom or molecule and knocks an electron out. By measuring the two outgoing electrons in coincidence, the kinematics of this process can be fully determined. The conservation of energy and momentum gives the binding energy ε_f and the momentum $\mathbf{p}$ of the electron in target orbital as

$$\varepsilon_f = E_0 - E_a - E_b \quad (1)$$

$$\mathbf{p} = \mathbf{p}_a + \mathbf{p}_b - \mathbf{p}_0 \quad (2)$$

where E_0, E_a, and E_b are kinetic energies and $\mathbf{p}_0$, $\mathbf{p}_a$ and $\mathbf{p}_b$ are momenta of the incident and two outgoing electrons respectively. In the present work, the

*Author to whom correspondence should be addressed. E-mail: xuck@ustc.edu.cn

experiment on iso-$C_2H_2Cl_2$ is performed using a high-sensitivity EMS spectrometer with a symmetric non-coplanar geometry, the details of which can be found elsewhere [21, 22]. During the experiment, the incident electron beam with the energy of 1200 eV plus binding energy collides with the target gas beam in the reaction region. The scattered and ejected electrons having equal polar angles (θ_a=θ_b=θ=45°) and energies (E_a=E_b) are detected in coincidence by a 90° sector spherical electrostatic analyzer with 2π azimuthal range followed by a position-sensitive detector, to obtain their energies and azimuthal angles simultaneously. The magnitude of the target orbital electron momentum $\mathbf{p}$ is then expressed as

$$\mathbf{p} = \left\{ \left(\sqrt{2}\mathbf{p}_a - \mathbf{p}_0 \right)^2 + \left[\sqrt{2}\mathbf{p}_a \sin\left(\varphi/2\right) \right]^2 \right\}^{1/2} \quad (3)$$

where φ is the relative azimuthal angle between the two outgoing electrons. From Eq.(1) and Eq.(3), the binding energy and momentum of the target electron can be determined. The energy and momentum resolution of the present EMS instrument are determined to be ∼1.1 eV (full width at half maximum (FWHM)) and ∼0.2 a.u. respectively, by measuring the ionization spectra and electron momentum distribution of Ar 3p orbital.

On the theoretical aspect, within the binary encounter approximation and plane wave impulse approximation (PWIA), the triple differential cross-section (TDCS) of (e, 2e) reaction for a molecule oriented randomly is given by [3]

$$\begin{aligned} \sigma_{\mathrm{EMS}} &= \frac{\mathrm{d}^3\sigma}{\mathrm{d}\Omega_1 \mathrm{d}\Omega_2 \mathrm{d}E_1} \\ &= (2\pi)^4 \frac{\mathbf{p}_a \mathbf{p}_b}{\mathbf{p}_0} f_{\mathrm{ee}} \sum_{\mathrm{av}} |\langle \mathbf{p}\, \psi_f | \psi_i \rangle|^2 \end{aligned} \quad (4)$$

where f_{ee} is the electron-electron Mott scattering cross-section, and $\sum_{\mathrm{av}}$ represents an average over initial neutral ψ_i and a sum over final ion ψ_f states. Under the weak-coupling approximation [1] and the target HF [1, 23−25] or Kohn-Sham (KS) approximation [26−28], the Eq.(4) can be simplified to

$$\sigma_{\mathrm{EMS}} \propto S_i^f \frac{1}{4\pi} \int |\phi_i(\mathbf{p})|^2 \, \mathrm{d}\Omega_p \quad (5)$$

Here S_i^f is called spectroscopic factor or pole strength (PS) which is the possibility of finding a one-hole configuration in the final ion state, and $\phi_i(\mathbf{p})$ is the one-electron momentum space canonical HF or KS orbital wave function in the neutral initial state for the ith electron corresponding to the orbital from which the target electron is ionized. The integral in Eq.(5) is referred to as the electron momentum profile (EMP).

In the present work, the EMPs for the valence shell of iso-$C_2H_2Cl_2$ have been calculated by the GAUSSIAN 09 program [29]. HF as well as DFT along with B3LYP functional methods is employed, with 6-31++G** and aug-cc-pVTZ basis sets. To be compared with the experiment, the calculations have been convoluted with the finite acceptance angles of the (e, 2e) spectrometer in both θ and φ ($\Delta\theta$=0.8°, $\Delta\varphi$=2.0°), using the Gaussian-weighted planar grid method [30]. The symmetry-adapted-cluster configuration-interaction (SAC-CI) general-R methods [31, 32] employing aug-cc-pVTZ basis set are also used to calculate the binding energy spectra of iso-$C_2H_2Cl_2$ for all the valence orbitals.

III. RESULTS AND DISCUSSION

A. Binding energy spectrum

For iso-$C_2H_2Cl_2$ molecule, there are 12 valence orbitals, which are classified into 4 inner-valence and 8 outer-valence orbitals. B3LYP calculation gives the electric configuration of iso-$C_2H_2Cl_2$ as

$$(\mathrm{core})^{14} \underbrace{(7a_1)^2 (5b_2)^2 (8a_1)^2 (9a_1)^2}_{\text{inner-valance}}$$
$$\underbrace{(6b_2)^2 (10a_1)^2 (2b_1)^2 (7b_2)^2 (11a_1)^2 (2a_2)^2 (8b_2)^2 (3b_1)^2}_{\text{outer-valence}}$$

The two-dimensional density map (2D map) of binding energy (in the range of 7−29.8 eV) and relative azimuthal angle (in the range from −50° to 50°) measured in the experiment are shown in FIG. 1(a), from which the momentum distributions and symmetries of Iso-$C_2H_2Cl_2$ valence orbitals can be clearly recognized. Integrating the 2D map over the complete azimuthal range, we obtain the total BES, which is shown in FIG. 1(b). Twelve Gaussian peaks (denoted as p1 to p12), corresponding to the ionization bands of the twelve valence orbitals, are employed to deconvolute the total BES. The position and width of each peak are determined with the help of the corresponding valence ionization energy and Franck-Condon width from high-resolution synchrotron radiation photoelectron spectra (SR PES) [14], with small adjustments to compensate the asymmetries of Franck-Condon profiles and the instrumental energy resolution. The fitted Gaussian peaks are drawn as blue dashed lines in FIG. 1(b), while the overall fitted spectra are plotted as red solid line. It is illustrated that the first peak in BES at 10.0 eV (band p1) is well resolved, which is contributed from the ionization of the highest occupied molecular orbital (HOMO) $3b_1$. The next seven bands at 11.6, 12.1, 12.5, 13.8, 14.3, 15.7, and 16.5 eV (p2 to p8) are assigned to the orbitals of $8b_2$, $2a_2$, $11a_1$, $7b_2$, $2b_1$, $10a_1$, and $6b_2$, respectively, all of which are outer-valence orbitals. The rest four bands in BES belong to the inner-valence shell, which are denoted as p9 (18.7 eV), p10 (23.4 eV), p11 (25.5 eV), and p12 (27.7 eV), corresponding to the

DOI:10.1063/1674-0068/cjcp1903059

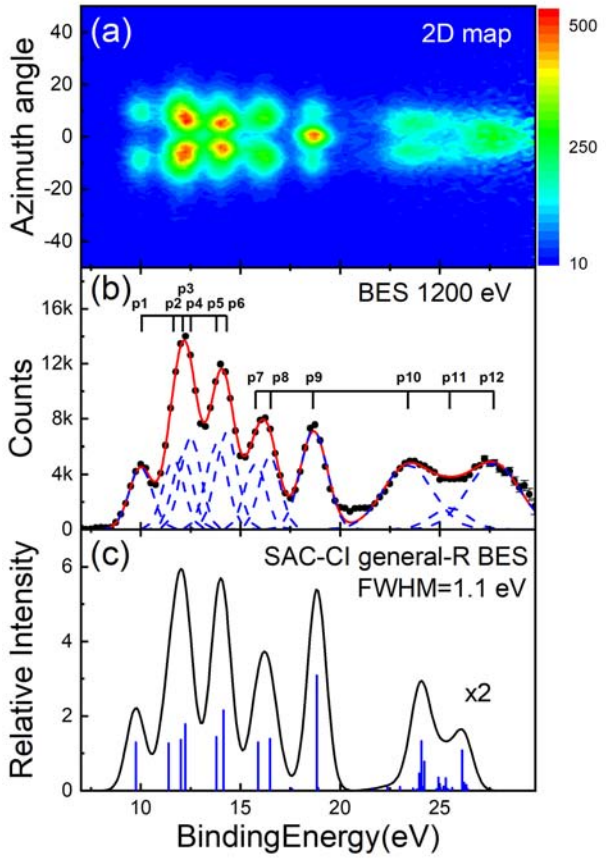

FIG. 1 (a) Two-dimensional electron density maps (2D maps) and (b) total binding energy spectra (BES) of iso-$C_2H_2Cl_2$. (c) Simulated BES by SAC-CI general-R. The vertical bars represent ionization transitions and their heights are pole strengths. The height of the vertical bars above 22 eV is multiplied by a factor of 2.

ionizations from $9a_1$, $8a_1$, $5b_2$, and $7a_1$ orbitals respectively. The ionization potentials (IPs) for the valence shells of iso-$C_2H_2Cl_2$ obtained in the present experiment are presented in Table I, as well as those from He I [13], SR PES [14] and previous EMS experiments [20].

For the sake of comparison, SAC-CI general-R calculations employing aug-cc-pVTZ basis set have been performed to calculate the IP and PS for each ionization transitions, which are also compiled in Table I. FIG. 1(c) shows the simulated BES by employing the calculated IPs convoluting with the instrumental function of 1.1 eV. The vertical bars represent ionization transitions and their heights are pole strengths. The height of the vertical bars above 22 eV is multiplied by a factor of 2. It can be seen that in the outer valence region, the SAC-CI general-R simulation reproduces the measured BES pretty well, while it fails to describe both the positions and intensities of the ionization bands from the three innermost valence orbitals.

B. Electron momentum profiles

Momentum-dispersed BES are converted from the 2D map according to Eq.(3), which are then deconvoluted with Gaussian function to obtain the experimental momentum profiles (XMPs) for the valence orbitals of iso-$C_2H_2Cl_2$. The deconvolution parameters are from the total BES and the XMPs are presented by the area under the fitted Gaussian peaks as a function of momentum $\mathbf{p}$. Statistical uncertainty as well as deconvolution error is taken into account to determine the error bar of each XMP datum. For comparison, theoretical momentum profiles (TMPs) are calculated by HF and DFT-B3LYP methods with 6-31++G** and aug-cc-pVTZ basis sets, using the Gaussian 09 program [29]. The spectrometer acceptance angles of $\Delta\theta$=0.8° and $\Delta\phi$=2.0° are folded into the TMPs using the Gaussian-weighted planar grid method [30]. A global normalization factor, which is determined from the comparison of the maximum in the momentum profile of HOMO ($3b_1$) obtained by experiment and B3LYP/aug-cc-pVTZ calculation, is employed to normalize the XMPs to the TMPs. The results are illustrated in FIGs. 2−4, where the XMPs are plotted as solid circles with error bars, and the TMPs are drawn as olive dot line for HF/6-31++G**, blue dash line for HF/aug-cc-pVTZ and red solid line for B3LYP/aug-cc-pVTZ respectively.

The first band p1 in BES is contributed from the ionization of $3b_1$ orbital (HOMO), the XMP and TMPs of which are given in FIG. 2(a). It should be noted that from the SAC-CI general-R calculation, the PS with respect to the ionization of HOMO is assumed to be 0.83. Therefore the global normalization factor is actually determined by normalizing the maximum of the XMP to that of the relevant TMP which is calculated by B3LYP/aug-cc-pVTZ and multiplied by a factor of 0.83, for the $3b_1$ orbital (HOMO). For the ionizations of other iso-$C_2H_2Cl_2$ valence orbitals, the PS is determined experimentally by comparing XMPs with TMPs (calculated by B3LYP/aug-cc-pVTZ) multiplied by the corresponding factors, which are listed in Table I. From FIG. 2(a), we can observe that all of the XMPs and TMPs show a typical p-type character with a maximum at about 0.75 a.u. The theoretical calculations reproduce the experimental data very well in large momentum region, but underestimate the XMPs in low momentum region. Such turn-up effects, which have been frequently reported in EMS studies on molecular π^* orbitals or atomic d orbitals, are usually ascribed to the distorted wave effects [33−36]. According to Ref.[20], the $3b_1$ orbital of iso-$C_2H_2Cl_2$ consists primarily of out-of-plane π bonding, but contains weak π^* overlaps as well. Therefore the observed turn-up effect in FIG. 2(a) may stem from the π^* component of this orbital, consequently being attributed to the distorted wave effects. As for the theoretical calculations, all the calculated curves show almost no difference from each other. This indicates that for the TMP calculations of this orbital,

DOI:10.1063/1674-0068/cjcp1903059

TABLE I Ionization potential (IP), assignment and pole strength (PS) for the ionization bands of iso-dichloroethylene valence shells.

Band	Assignment	Present EMS		SAC-CI general-R		EMS [20]	He I PES [13]	SR PES [14]
		IP/eV	PS	IP/eV	PS	IP/eV	IP/eV	IP/eV
p1	$3b_1^{-1}$	10.0	0.83	9.76	0.83	10.0	10.00	10.0
p2	$8b_2^{-1}$	11.6	0.83	11.4	0.83		11.67	11.6
p3	$2a_2^{-1}$	12.1	0.83	12.0	0.82	12.1	12.17	12.1
p4	$11a_1^{-1}$	12.5	0.83	12.2	0.82		12.51	12.5
p5	$7b_2^{-1}$	13.8	0.83	13.8	0.82	13.5	13.70	13.8
p6	$2b_1^{-1}$	14.3	0.78	14.2	0.79	14.5	14.24	14.3
p7	$10a_1^{-1}$	15.7	0.83	15.9	0.80	15.7	16.27	15.7
p8	$6b_2^{-1}$	16.5	0.79	16.5	0.78	17.0	16.27	16.3
p9	$9a_1^{-1}$	18.7	0.68	18.8	0.74	18.6		18.6
p10	$8a_1^{-1}$	23.4	0.83	23.0−24.4	0.57	23.2		23.2
p11	$5b_2^{-1}$	25.5	0.19	24.4−25.4	0.10	25.5		25.5
p12	$7a_1^{-1}$	27.7	0.28	26.0−26.9	0.09	27.7		27.7

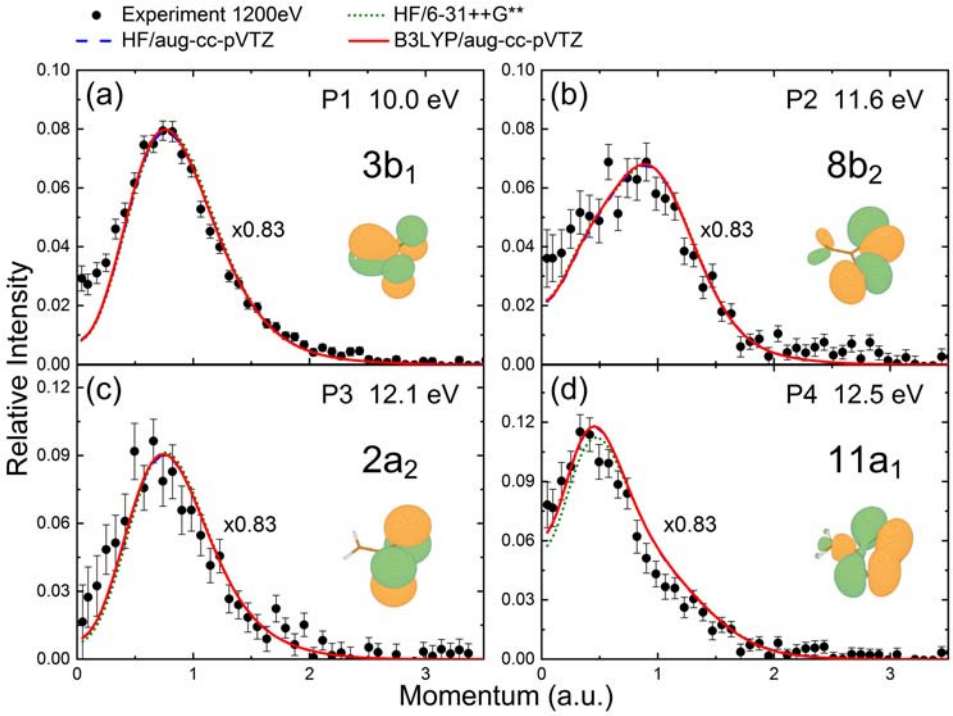

FIG. 2 Experimental and theoretical electron momentum profiles for the ionization bands from p1 to p4, which are corresponding to the iso-$C_2H_2Cl_2$ outer-valence orbitals of $3b_1$ (a), $8b_2$ (b), $2a_2$ (c) and $11a_1$ (d) respectively. The incident energy is 1200 eV plus binding energy. The calculated electron density distributions of these orbitals are shown as the inserts.

6-31++G** basis set is large enough, and the selection of methods (HF or B3LYP) has little influence.

The XMPs and TMPs of the p2 ($8b_2$), p3 ($2a_2$), and p4 ($11a_1$) ionization bands are shown in FIG. 2 (b), (c), and (d) respectively, which have not been reported before. It is observed that both the experimental and calculated momentum profiles of these orbitals display mainly p-type characters, with the maximums at about 0.90, 0.75, and 0.45 a.u., corresponding to $8b_2$, $2a_2$ and $11a_1$ orbitals respectively. All the calculations for each of these three orbitals are shown to be consistent with each other and fit the experimental data very well. The PS values for these three ionization bands are determined experimentally, all of which are 0.83, being equal to that for HOMO ($3b_1$).

The next four ionization bands p5−p8 are assigned to the outer-valence orbitals of $7b_2$, $2b_1$, $10a_1$ and $6b_2$ respectively. The XMPs and TMPs of $7b_2$ and $2b_1$ orbitals have not been reported before, while those of $10a_1$ and $6b_2$ orbitals were investigated by Chuaqui *et*

DOI:10.1063/1674-0068/cjcp1903059

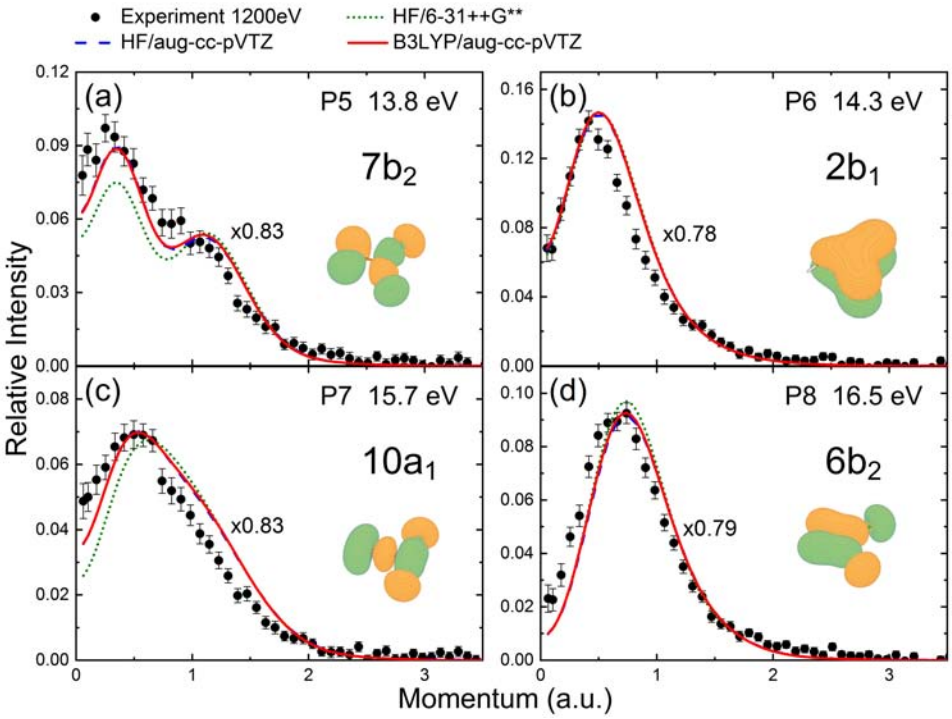

FIG. 3 Experimental and theoretical electron momentum profiles for the ionization bands from p5 to p8, which are corresponding to the iso-$C_2H_2Cl_2$ outer-valence orbitals of $7b_2$ (a), $2b_1$ (b), $10a_1$ (c) and $6b_2$ (d) respectively. The incident energy is 1200 eV plus binding energy. The calculated electron density distributions of these orbitals are shown as the inserts.

al. [20]. However, only the combined momentum profile is given in Ref.[20], and significant discrepancy between the experiment and calculations was observed. In the present work, the measured momentum profiles of $7b_2$, $2b_1$, $10a_1$ and $6b_2$ orbitals are shown in FIG. 3 (a)−(d) respectively, together with the theoretical calculations. In FIG. 3(a), both the XMPs and TMPs of $7b_2$ orbital exhibit a double p-type distribution with the first maximum at about 0.40 a.u. and the second maximum at about 1.15 a.u. It is observed that the calculations employing whether HF or B3LYP methods with aug-cc-pVTZ basis set resemble the XMP pretty well, but the one calculated with 6-31++G** basis set obviously underestimates the XMP in the region below 1.15 a.u. This indicates that adequately large basis set is of most importance in the calculations for $7b_2$ orbital. The PS for this ionization band is also determined to be 0.83. The momentum distributions of $2b_1$ orbital are illustrated in FIG. 3(b), which shows a p-type character with a maximum at about 0.50 a.u. All theoretical calculations exhibit almost no difference from each other, and reproduce the XMP well. The PS for this band is determined experimentally to be 0.78. The last two outer-valence orbitals are $10a_1$ and $6b_2$, the XMP and TMPs of which are shown in FIG. 3 (c) and (d) respectively. It is observed that for both orbitals, B3LYP and HF calculations with aug-cc-pVTZ basis sets show no difference. However, the discrepancy between the calculations with large basis set (aug-cc-pVTZ) and relatively small basis set (6-31++G**) are obvious for $10a_1$ but slight for $6b_2$ orbitals. The general agreement between the XMP and TMPs are fairly well for both orbitals, and the discrepancy may be due to the electron correlation effect, distorted wave effect or the uncertainty in the deconvolution procedure. The PSs for these two bands are determined to be 0.83 and 0.79 respectively.

There are four inner-valence orbitals of iso-$C_2H_2Cl_2$, which are $9a_1$, $8a_1$, $5b_2$ and $7a_1$. In the present work, the BES range covers the ionization energies of all the inner-valence orbitals. Therefore the XMPs of these orbitals are obtained and displayed in FIG. 4 (a)−(d) respectively, together with the calculated TMPs. In general, for each of the four orbitals, all the TMPs show almost no difference from each other, indicating the independence of the calculations on the method as well as the basis set larger than 6-31++G**. For $9a_1$ orbital, the TMPs fit the XMP pretty well, demonstrating an sp-type character with the second maximum at about 0.80 a.u., as shown in FIG. 4(a). The momentum distributions of $8a_1$ orbital are shown in FIG. 4(b), showing a p-type character with the maximum at about 0.55 a.u. The TMPs reproduce the XMP well only in the peak region from 0.4 a.u. to 1.2 a.u., but underestimate it in the else region. As for $5b_2$ orbital in FIG. 4(c), the calculations are observed to well resemble the experimental data below 1.5 a.u., which also show a p-type distribution with the maximum at about 0.55 a.u. How-

DOI:10.1063/1674-0068/cjcp1903059

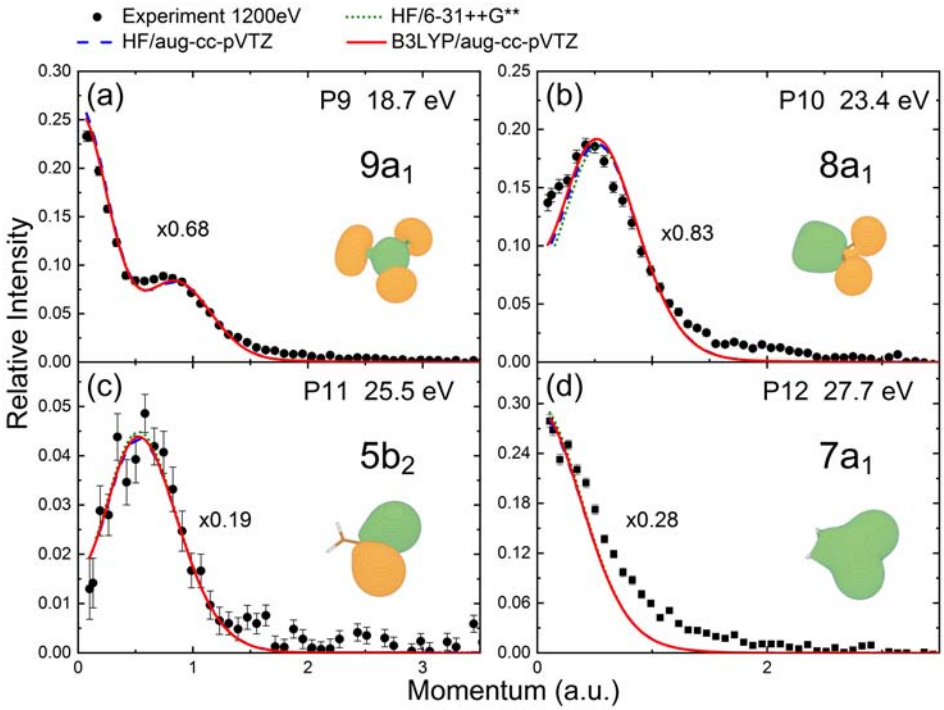

FIG. 4 Experimental and theoretical electron momentum profiles for the ionization bands from p9 to p12, which are corresponding to the iso-$C_2H_2Cl_2$ inner-valence orbitals of $9a_1$ (a), $8a_1$ (b), $5b_2$ (c) and $7a_1$ (d) respectively. The incident energy is 1200 eV plus binding energy. The calculated electron density distributions of these orbitals are shown as the inserts.

ever, deviations between the theoretical curve and the experimental data can be found in the higher momentum region (above 1.5 a.u.). The XMP and TMPs of the last inner-valance orbital $7a_1$ are shown in FIG. 4(d). Although all the momentum profiles exhibit s-type character, the TMPs fit the XMP not so well. The discrepancies between the calculation and experiment for $8a_1$, $5b_2$ and $7a_1$ orbitals are probably due to the breakdown of the PWIA, since in the inner-valence shell the distorted wave effect becomes more and more important. Besides, from the SAC-CI general-R simulated BES shown in FIG. 1(c), we can observe several satellites overlapping in the energy range covering the ionization bands p10−p12, corresponding to these three most-inner valance orbitals. This may be another reason why the calculated EMDs do not agree with the experimental data very well for $8a_1$, $5b_2$ and $7a_1$ orbitals. The PSs for the ionization of all the inner-valence orbitals are determined experimentally, which are 0.68 ($9a_1$), 0.83 ($8a_1$), 0.19 ($5b_2$) and 0.28 ($7a_1$) respectively.

It is worth noting that from the electron density distributions displayed in the inserts of FIG. 2(c) and FIG. 4(c), the orbitals $2a_2$ and $5b_2$ of iso-$C_2H_2Cl_2$ are mainly Cl 3p and 3s lone-pair electrons respectively. Recent researches have revealed that due to the multiple atomic centers participating in the bonding or antibonding interaction, the EMPs of lone-pair orbitals in molecules such as CF_4 [37], SF_6 [6, 38], CCl_4 [39], C_3H_8 [40] *etc.* will be influenced significantly by the interference effects (also referred as bond oscillations). Under the linear combination of atomic orbitals approximation, the TDCS of EMS for lone-pair orbital can be written as

$$\sigma_{\mathrm{EMS}}(p) \propto \sigma_{\mathrm{AO}}(p)\, I(p) \tag{6}$$

Here $\sigma_{\mathrm{AO}}(p)$ is the TDCS for the atomic orbital (AO) of an isolated atom corresponding to the lone-pair electrons, and $I(p)$ is referred to as the interference factor (IF). For $2a_2$ and $5b_2$ orbitals of iso-$C_2H_2Cl_2$, the IF can be deduced as [37, 38]

$$\mathrm{IF} = 1 + a_0 \frac{\sin(pR)}{pR} + a_2 \frac{3\left[\sin(pR) - pR\cos(pR)\right] - (pR)^2 \sin(pR)}{(pR)^2} \tag{7}$$

where a_0 and a_2 are the coefficients of the spherical Bessel functions of order 0 and 2 respectively, and R is the distance between two Cl nuclei. According to B3LYP/aug-cc-pVTZ calculation, these three parameters are determined to be -1 for both of a_0 and a_2, and 5.51 a.u. for R respectively. In FIG. 5 (a) and (b), the EMPs of $2a_2$ and $5b_2$ orbitals are compared with those of the corresponding AOs respectively. In each figure, the XMP and TMP of iso-$C_2H_2Cl_2$ lone-pair orbital are shown as black solid circle and red solid line respectively, the IF is denoted as olive dot dash line, and the

DOI:10.1063/1674-0068/cjcp1903059

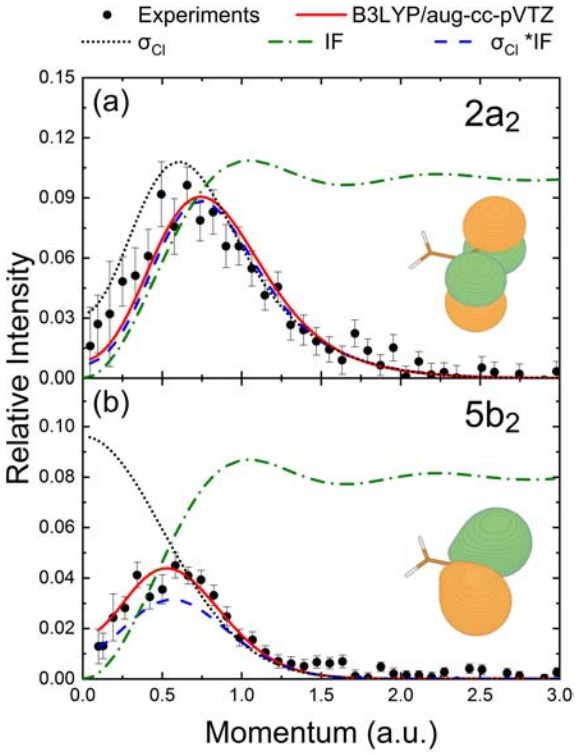

FIG. 5 Comparison of the EMPs for (a) $2a_2$ lone-pair orbital with Cl 3p AO and (b) $5b_2$ lone-pair orbital with Cl 3s AO. The XMPs and TMPs of iso-$C_2H_2Cl_2$ lone-pair orbitals are shown as black solid circle and red solid line respectively, the IF is denoted as olive dot dash line, and the TMPs of Cl AOs and that multiplied by IF are plotted as black dot line and blue dash line respectively.

TMP of respective Cl AO and that multiplied by IF are plotted as black dot line and blue dash line respectively. The TMPs of the Cl 3p and 3s AOs are calculated by B3LYP method employing aug-cc-pVTZ basis set, into which the present instrumental momentum resolution is folded for comparison. In FIG. 5(a), it is shown that both of the EMPs for $2a_2$ orbital and Cl 3p AO exhibit p-type character, but the peak maximum in EMP for Cl 3p AO shifts to lower momentum compared with that for $2a_2$ orbital. Multiplied by IF, the EMP of Cl 3p AO fits that of $2a_2$ orbital very well. In FIG. 5(b), we can observe that the EMP of $5b_2$ orbital exhibits p-type character, whereas that of Cl 3s AO shows s-type distribution. Being modulated by IF, which is illustrated to drop to zero as the momentum decreases to the origin in the momentum region below 1.0 a.u., the EMP of Cl 3s AO then displays p-type character, reproducing that of $5b_2$ orbital in shape pretty well but underestimating it in intensity. From the electron density distributions shown in the inserts of FIG. 5, we can observe that the $2a_2$ orbital is a relatively pure Cl lone-pair orbital, whereas the $5b_2$ orbital is slightly contributed from the C−Cl bonding electrons. This may explain the discrepancy of EMP between the Cl 3s AO multiplied with IF and the $5b_2$ orbital in FIG. 5(b). These results indicate that the interference effects will greatly influence the momentum distributions of Cl lone-pair orbitals in iso-$C_2H_2Cl_2$ valence shell.

IV. CONCLUSION

We report the EMS studies on all of the iso-$C_2H_2Cl_2$ valence orbitals at incident energy 1.2 keV plus binding energy. The two-dimensional electron density map with respect to binding energy and azimuthal angle is measured, and the XMP of each valence orbital is obtained through deconvolution process. The TMPs are calculated by both HF and DFT-B3LYP methods, employing 6-31++G** and aug-cc-pVTZ basis sets. The comparison of TMPs indicates that the calculations employing B3LYP method and HF method with aug-cc-pVTZ basis set show almost no difference from each other. For most of the iso-$C_2H_2Cl_2$ valence orbitals, 6-31++G** basis set is proven to be large enough for the calculations, which fits the XMP as well as the calculations with aug-cc-pVTZ. However, for $11a_1$, $7b_2$ and $10a_1$ orbitals, the TMPs calculated with 6-31++G** show obvious discrepancies with the XMPs, while those calculated with aug-cc-pVTZ still fit the experimental data very well. It is observed that the momentum profiles of $2a_2$ and $5b_2$ orbitals which belong to Cl 3p and 3s lone-pair orbitals respectively, are significantly influenced by interference effects.

V. ACKNOWLEDGMENTS

This work was supported by the National Natural Science Foundation of China (No.11534011) and the National Key Research and Development Program of China (No.2017YFA0402300). The authors also gratefully acknowledge Professor C. E. Brion at the University of British Columbia (UBC) in Canada for giving us the HEMS programs.

[1] I. E. McCarthy and E. Weigold, Rep. Prog. Phys. **54** 789 (1991).
[2] M. A. Coplan, J. H. Moore, and J. P. Doering, Rev. Mod. Phys. **66**, 985 (1994).
[3] E. Weigold and I. E. McCarthy, *Electron Momentum Spectroscopy*, New York: Kluwer Academic/Plenum Publishers, (1999).
[4] E. L. Wang, Y. F. Shi, X. Shan, H. J. Yang, W. Zhang, and X. J. Chen, Chin. J. Chem. Phys. **27**, 503 (2014).
[5] Y. F. Shi, X. Shan, E. L. Wang, H. J. Yang, W. Zhang, and X. J. Chen, Chin. J. Chem. Phys. **28**, 35 (2015).
[6] M. F. Zhao, X. Shan, J. Yang, E. L. Wang, S. S. Niu, and X. J. Chen, Chin. J. Chem. Phys. **28**, 539 (2015).
[7] M. Li, X. Shan, S. S. Niu, Y. G. Tang, F. Wu, C. K. Xu, and X. J. Chen, Chin. J. Chem. Phys. **29**, 645 (2016).

DOI:10.1063/1674-0068/cjcp1903059

[8] A. O. Bawagan, R. Müller-Fiedler, C. E. Brion, E. R. Davidson, and C. Boyle, Chem. Phys. **120**, 335 (1988).
[9] Z. H. He, X. Yang, X. J. Zhou, and K. T. Leung, Surf. Sci. **547**, L840 (2003).
[10] Q. J. Zhang, B. Li, Q. H. Yuan, B. H. Li, Z. F. Liu, and L. Chen, Phys. Chem. Chem. Phys. **13**, 7121 (2011).
[11] Z. H. He, Q. Li, and K. T. Leung, Surf. Sci. **600**, 514 (2006).
[12] G. Bieri, L. Åsbrink, and W. Von Niessen, J. Electron Spectrosc. Relat. Phenom. **23**, 281 (1981).
[13] K. Kimura, S. Katsumata, Y. Achiba, T. Yamazaki, and S. Iwata, *Handbook of HeI Photoelectron Spectra of Fundamental Organic Molecules Halsted*, New York: Halsted Press, (1981).
[14] J. F. Ying and K. T. Leung, J. Electron Spectrosc. Relat. Phenom. **63**, 75 (1993).
[15] R. Locht, D. Dehareng, and B. Leyh, J. Phys. Commun. **1**, 055030 (2017).
[16] A. Cassuto, M. B. Hugenschmidt, P. Parent, C. Laffon, and H. G. Tourillon, Surf. Sci. **310**, 390 (1994).
[17] D. Cèolin, O. Travnikova, Z. Bao, A. Kivimäki, S. Carniato, and M. N. Piancastelli, J. Electron Spectrosc. Relat. Phenom. **184**, 24 (2011).
[18] D. Cèolin, O. Travnikova, Z. Bao, F. F. Guimarães, M. S. da Costa, Y. Velkov, N. Sisourat, S. Carniato, M. Simon, and M. N. Piancastelli, J. Electron Spectrosc. Relat. Phenom. **185**, 252 (2012).
[19] K. Ohno, N. Kishimoto, and H. Yamakado, J. Phys. Chem. **99**, 9687 (1995).
[20] M. H. Chuaqui, L. Mei, C. P. Mathers, M. L. Allison, J. F. Ying, and K. T. Leung, J. Chem. Phys. **102**, 90 (1995).
[21] Q. G. Tian, K. D. Wang, X. Shan, and X. J. Chen, Rev. Sci. Instrum. **82**, 033110 (2011).
[22] Y. G. Tang, X. Shan, J. Yang, S. S. Niu, Z. Zhang, N. Watanabe, M. Yamazaki, M. Takahashi, and X. J. Chen, J. Phys. Chem. A **120**, 6855 (2016).
[23] K. T. Leung and C. E. Brion, Chem. Phys. **96**, 241 (1985).
[24] A. Minchinton, J. P. D. Cook, E. Weigold, and W. von Niessen, Chem. Phys. **113**, 251 (1987).
[25] M. Takahashi, R. Ogino, and Y. Udagawa, Chem. Phys. Lett. **288**, 714 (1998).
[26] P. Duffy, D. P. Chong, M. E. Casida, and D. R. Salahub, Phys. Rev. A **50**, 4707 (1994).
[27] M. E. Casida, Phys. Rev. A **51**, 2005 (1995).
[28] P. Duffy, Can. J. Phys. **74**, 763 (1996).
[29] M. Frisch, G. Trucks, H. Schlegel, G. Scuseria, M. Robb, J. Cheeseman, G. Scalmani, V. Barone, B. Mennucci, and G. Petersson, *Gaussian 09*, Wallingford, CT: Gaussian Inc, (2009).
[30] P. Duffy, M. E. Cassida, C. E. Brion, and D. P. Chong, Chem. Phys. **159**, 347 (1992).
[31] M. Ehara and H. Nakatsuji, Spectroc. Acta Pt. A Molec. Biomolec. Spectr. **55**, 487 (1999).
[32] M. Ishida, K. Toyota, M. Ehara, and H. Nakatsuji, Chem. Phys. Lett. **347**, 493 (2001).
[33] M. J. Brunger, I. E. McCarthy, and E. Weigold, Phys. Rev. A **59**, 1245 (1999).
[34] X. G. Ren, C. G. Ning, J. K. Deng, S. F. Zhang, G. L. Su, F. Huang, and G. Q. Li, Phys. Rev. Lett. **94**, 163201 (2005).
[35] C. G. Ning, X. G. Ren, J. K. Deng, G. L. Su, S. F. Zhang, and G. Q. Li, Phys. Rev. A **73**, 022704 (2006).
[36] Y. G. Tang, X. Shan, S. S. Niu, Z. H. Liu, E. L. Wang, N. Watanabe, M. Yamazaki, M. Takahashi, and X. J. Chen, J. Phys. Chem. A **121**, 277 (2017).
[37] N. Watanabe, X. J. Chen, and M. Takahashi, Phys. Rev. Lett. **108**, 173201 (2012).
[38] N. Watanabe, M. Yamazaki, and M. Takahashi, J. Electron Spectrosc. Relat. Phenom. **209**, 78 (2016).
[39] N. Watanabe, K. Katafuchi, M. Yamazaki, and M. Takahashi, Eur. Phys. J. D **70**, 268 (2016).
[40] S. S. Niu, Y. G. Tang, Z. H. Liu, X. Shan, and X. J. Chen, J. Electron Spectrosc. Relat. Phenom. **229**, 52 (2018).

DOI:10.1063/1674-0068/cjcp1903059